Large Piezoelectric Response of van der Waals Lavered Solids

Sukriti Manna ^{1,3}, Prashun Gorai^{2,3}, Geoff L. Brennecka², Cristian V. Ciobanu ¹, and Vladan Stevanovi´c^{2,3}

¹Dept. of Mechanical Engineering, Colorado School of Mines, Golden, Colorado 80401, USA

²Dept. of Metallurgical and Materials Engineering,

Colorado School of Mines, Golden, Colorado 80401, USA

³National Renewable Energy Laboratory, Golden, CO 80401, USA

(Dated: May 1, 2018)

The bulk piezoelectric response, as measured by the piezoelectric modulus tensor (δ) , is determined by a combination of charge redistribution due to strain and the amount of strain produced by the application of stress (stiffness). Motivated by the notion that less stiff materials could exhibit large piezoelectric responses, herein we investigate the piezoelectric modulus of van der Waals-bonded quasi-2D ionic compounds using first-principles calculations. From a pool of 869 known binary and ternary quasi-2D materials, we have identified 135 non-centrosymmetric crystals of which 48 systems are found to have δ components larger than the longitudinal piezoelectric modulus of AlN (a common piezoelectric for resonators), and three systems with the response greater than that of PbTiO $_3$, which is among the materials with largest known piezoelectric modulus. None of the identified materials have previously been considered for piezoelectric applications. Furthermore, we find that large δ components always couple to the deformations (shearing or axial) of van der Waals "gaps" between the layers and are indeed enabled by the weak intra-layer interactions.

I. MTRODUCTION

Coupling between the mechanical degrees offreedom and the electric polarization in a solid. a hallmark of piezoelectric materials, has found use in applications that range from sensors, resonators, motors, and actuators, to high-resolution ultrasound devices and miniature filters for cellular communications. 1-3 Interestingly, only about 10 piezoelectric materials, including SiQ (quartz), LiTaO₃, LiNbO₃, PZT (lead zirconate titanate)-based, BaTiO₃-based, (K,Na)NbO₃-based, Bi₄Ti₃O₁₂-based, AIN, and ZnO, are technologically relevant and cover virtually all of these applications. 4-6 Expanding the pool of known piezoelectric materials would help broaden the range of applications and allow earth-abundant and non-toxic replacements for materials that are presently Furthermore, it would offer more cost- and performance-effective choices beyond a relatively limited set of materials that are at present used for their piezoelectric properties.

The need for new piezoelectrics was recognized before and was the main motivation behind recent computational efforts in high-throughput screening of inorganic materials for piezoelectric performance. These include the work on perovskite alloys, 8,9 and creation of a database of piezoelectric properties of compounds. Materials with reduced dimensionality, such as 2D mono- and multi-layers have also been investigated recently. $^{11-16}$ In virtually all of these works, the quantity of interest was the piezoelectric coefficient tensor e_{ij} , which relates the polarization P_i to strain $_j$, 17,18 (in Voigt notation, 19 P_i = $_j$ e_{ij} $_j$) and is typically obtained from first-principles calculations.

In this work, we also apply first-principles calculations to screen for candidate piezoelectrics, but instead of the piezoelectric coefficient tensor we consider the piezoelectric modulus tensor d_{ij} , which relates the induced polar-

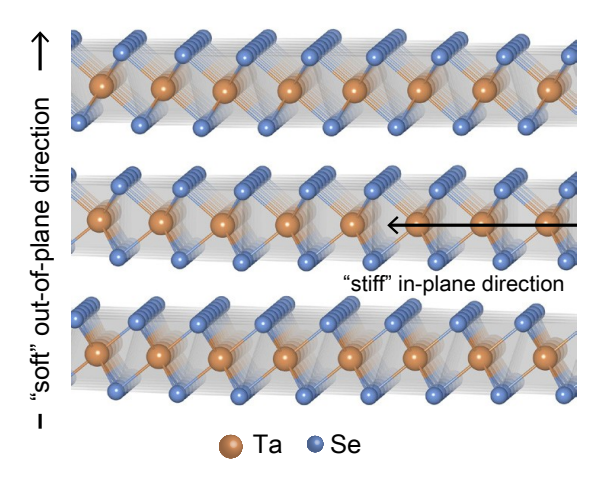


FIG. 1. Illustration of a quasi-2D material (TaSe₂), showing the atomic structure of the layers and the van der Waals spacing between them.

ization to the applied stress, $P_i = \frac{P}{j} d_{ij} \sigma_j$.17,18 The advantage of using d_{ij} is in that it represents an important figure of merit in a wide range of technological applications 1,2 and is a more commonly measured piezoelectric property, especially for materials in the thin film form. Because the induced polarization depends on the applied stress through a combination of the charge redistribution due to strain and the amount of strain that is produced by the applied stress, the piezoelectric modulus tensor d_{ij} depends on both the piezoelectric coefficient tensor e_{ij} and the elastic tensor C_{ij} as:

$$d_{ij} = \sum_{k=1}^{X^6} e_{ik} (C^{-1})_{kj}.$$
 (1)

From equation (1), we can infer that large piezoelectric modulus d_i can be expected in materials with large large

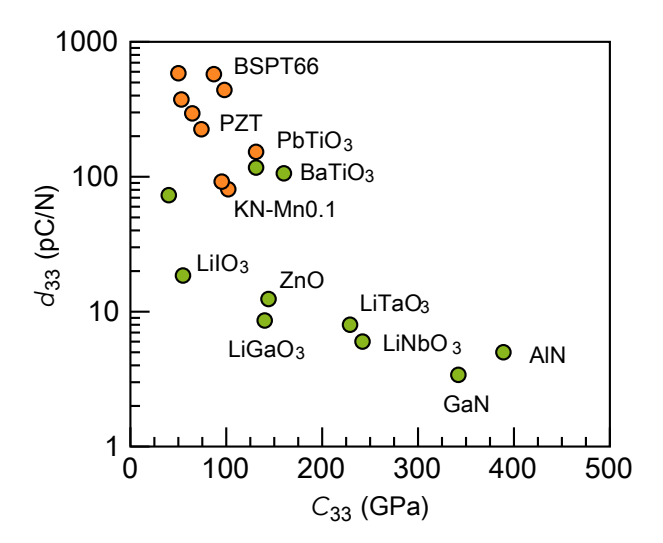


FIG. 2. Correlation between experimentally measured longitudinal piezoelectric modulus (d_{33}) and their elastic modulus (C_{33}). Green circles denote data from either single crystals or single-crystal, single-domain samples in case of ferroelectric materials. Orange circles denote polycrystalline samples. Data is sourced from Refs. 1,2,20–25.

 e_{ij} , but also in systems with low stiffness \mathcal{G} . Softer (less stiff) materials can exhibit large piezoelectric response, as measured by d_{ij} , compared to stiffer materials with similar e_{ij} . This is illustrated in Figure 2, where we notice less stiff materials overall exhibit larger piezoelectric responses in the corresponding direction.

For this reason, we concentrate our investigation on layered (quasi-2D) van der Waals bonded solids, which can be expected to have relatively low stiffness in the out-of-plane direction due to the presence of weak van der Waals (vdW) interactions between the layers. The questions we are addressing are: (a) whether materials that belong to this class and exhibit strong piezoelectric response (*q*) can be found, and (b) if this is true, what is the role of vdW interactions in enabling the strong response. To our knowledge, these questions have not been previously addressed in a systematic way.

Our results confirm the expectations. The search has revealed a number of quasi-2D materials with relatively large d_{ij} components. Out of 869 considered binary and ternary layered VdW systems, we have identified 135 non-centrosymmetric crystals. Out of those we find more than one third (48 compounds) exhibit piezoelectric moduli greater than that of AlN (d_{33} =5.5 pC/N), a commonly used piezoelectric material in resonator applications. In addition, we found three layered systems with piezoelectric moduli even larger than that of PbTiO ₃ (d_{33} =119 pC/N), another established piezoelectric material known for its very large response. It is important to note that none of these vdW systems have been considered previously for piezoelectric applications.

After performing a thorough analysis of the coupling between various stress and ϕ components, we find that

in all of these systems, large piezoelectric response is always coupled to the stress components that imply deformations (axial or shear) of the van der Waals "gaps" between the layers. This is consistent with the fact that the softest elastic constants are related to these deformations. Ultimately, our results point to the layered vdW systems as a rich chemical space for finding new piezoelectric materials, and introduce elastic properties as additional design criteria for finding materials with large piezoelectric modulus.

II. COMPUTATIONAL METRODOLOGY

In this section, we discuss the details of the computational methodology used in our calculations, broadly divided into three main subsections. The first subsection describes the procedure for identifying quasi-2D structures from the Inorganic Crystal Structure Database (ICSD). 26,27 Next, we describe the drawbacks of GGA exchange correlation functionals for predicting the properties of layered materials and our approach to overcome this issue. Then, we provide detailed descriptions of our workflow for evaluating the piezoelectric modulus tensors (δ) of quasi-2D solids.

A. Automated Identification of Quasi 2D Materials

An essential component of this work is the identification of layered (quasi-2D) vdW materials from ICSD. To accomplish this, we extend the applications of our previously-developed procedure for automated identification of the binary quasi-2D materials from the ICSD to include ternary chemistries. Similar algorithms have been developed and used for the purpose of broad identification of vdW bonded layered systems by others, including the work of Ashton *et al.*, ²⁹ Mounet *et al.*, ³⁰ and Cheon *et al.*³¹

Our procedure relies on a slab cutting routine and bond counting. In the first step, we cut out stoichiometric slabs of a certain thickness for all symmetry inequivalent sets of Miller indices (hkl) within a certain range $(-3 \le h, k, l \le 3)$. Next, for each slab we find the terminations of its surfaces that minimize the number of broken bonds by translating surface atoms from one side of the slab to the other using appropriate lattice vectors. We then count the (minimal) number of broken bonds, i.e., the under-coordination, of the surface atoms. The condition of quasi low-dimensional crystals then implies the existence of (hkl) directions for which the corresponding slabs do not have any under-coordinated atom relative to their bulk coordination in the first shell. is exactly one such (hkl), the material is a layered material with relatively large spatial gaps separating individual layers. If the number of directions is larger than one, then the corresponding systems are of lower dimensionality, quasi-1D for two such directions and molecular

crystals for larger than two. If there are no such directions, the structure is then a connected 3D structure without large spatial gaps.

In Ref. 28 we demonstrated the success of our algorithm in searching complex quasi-2D materials, including those with layer stacking in oblique directions, materials with corrugated, accordion-like layers, and those with individual layers composed of multiple atomic layers. Using the described automated algorithm, we have in this work considered 3500 binary and 8000 additional ternary compounds from the ICSD and classified them into layered (quasi-2D) and not layered materials. We restricted our search to stoichiometric and ordered systems that do not contain rare earth elements and have 50 of less atoms in the unit cell. From our calculations, we have identified 426 binary and 443 ternary quasi-2D compounds. A full list of these materials can be found in supplementary information with their ICSD id.

3. Calculating Piezoelectric Properties of Quasi-2D Materials

In quasi-2D structures considered in this work, the individual layers are held together by relatively weak vdW interactions. The standard exchange-correlation functionals typically employed in density functional (DFT) calculations, including the calculations of elastic and piezoelectric properties, are known to fail to describe the vdW interactions. This is evident from relatively large errors in the out-of-plane lattice constants and the associated elastic properties.³² To overcome this issue. we employed a vdW-corrected functional (optB86) as implemented in VASP (Vienna Ab-initio Simulation Package) code^{33,34} to calculate the lattice parameters, elastic, and piezoelectric properties of quasi-2D materials. 35,3 To evaluate the piezoelectric coefficient tensors, we utilize the VASP implementation of the density functional perturbation theory (DFPT) ^{37–39} calculations. A relatively large plane wave cutoff energy of 540 eV is used for structural relaxation, calculation of elastic tensors, and piezoelectric coefficient tensors A dense k-point grid, defined by $n_{\text{atoms}} \times n_{\text{kpoints}} \approx 1000$, where n_{atoms} is number of atoms in the primitive cell and n_{kpoints} is the number of k-points, is employed. In all our calculations, a very high tolerance of 10⁻⁸ eV for energy convergence is used, which is an important consideration for conducting DFPT calculations. ¹⁰ For calculation of elastic tensors we use a finite difference method. Here, the full elastic tensor is calculated by conducting six finite distortions of the lattice and obtaining elastic constants (C ij) from the stress-strain relationship. 40,41

The importance of incorporating vdW-corrections is illustrated in Figure 3, where we notice significant improvement in predicting elastic constants, particularly C_{33} and C_{44} , with vdW-corrected functional (optB86) 35,36 compared to standard GGA-PBE functional. 42 The GGA-PBE predicted elastic constants

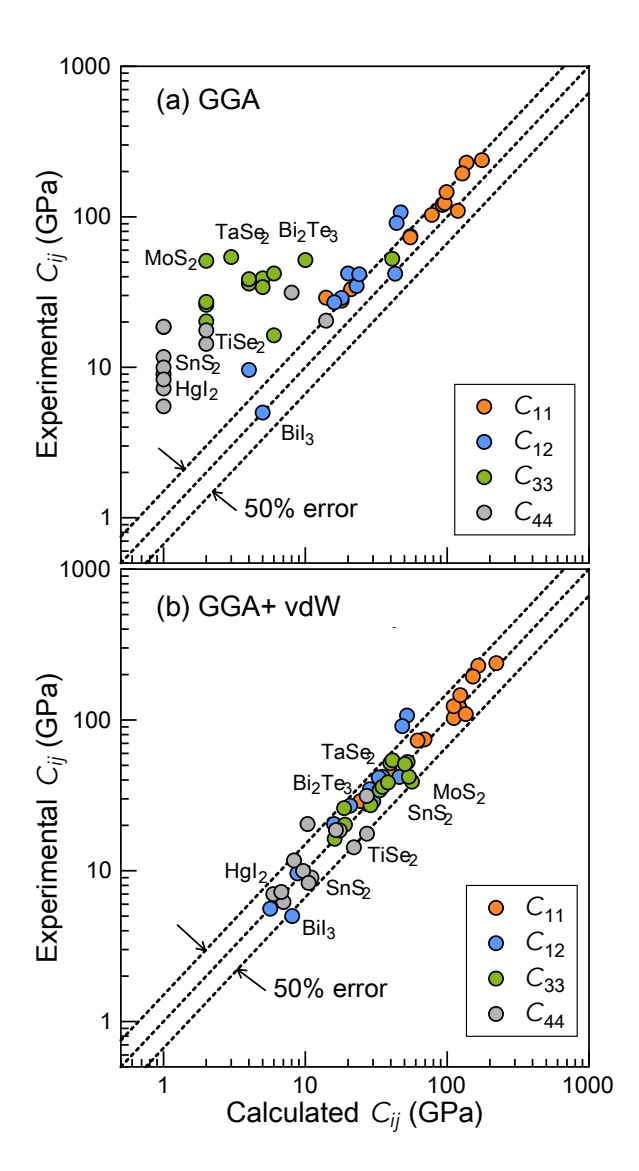


FIG. 3. Elastic constants of quasi-2D materials calculated with (a) GGA and (b) vdW-corrected functional. The calculated values are compared with experimental ones. The calculations with the vdW-corrected functional are all within 50% error relative to the measurements. Details of measurement techniques, measurement temperatures, etc., are provided in the supplementary informations.

are sourced from Ref. 43A more detailed analysis of the data presented in Figure 3 reveals that the GGA-PBE is still better in predicting in-plane elastic coefficients C_{11} and C_{12} , but the error in reproducing C_{33} and C_{44} is a factor of 10 or larger. This is due the fact that these particular two elastic constants are directly related to the deformations of the spatial gaps between the layers and the failure of GGA-PBE in reproducing relatively weak vdW interactions. The comparison of predicted properties with GGA-PBE and vdW-corrected functional is limited only to the elastic constants (Figure 3); the lack of experimental data on piezoelectric properties of quasi-2D materials prevented us from making similar compar-

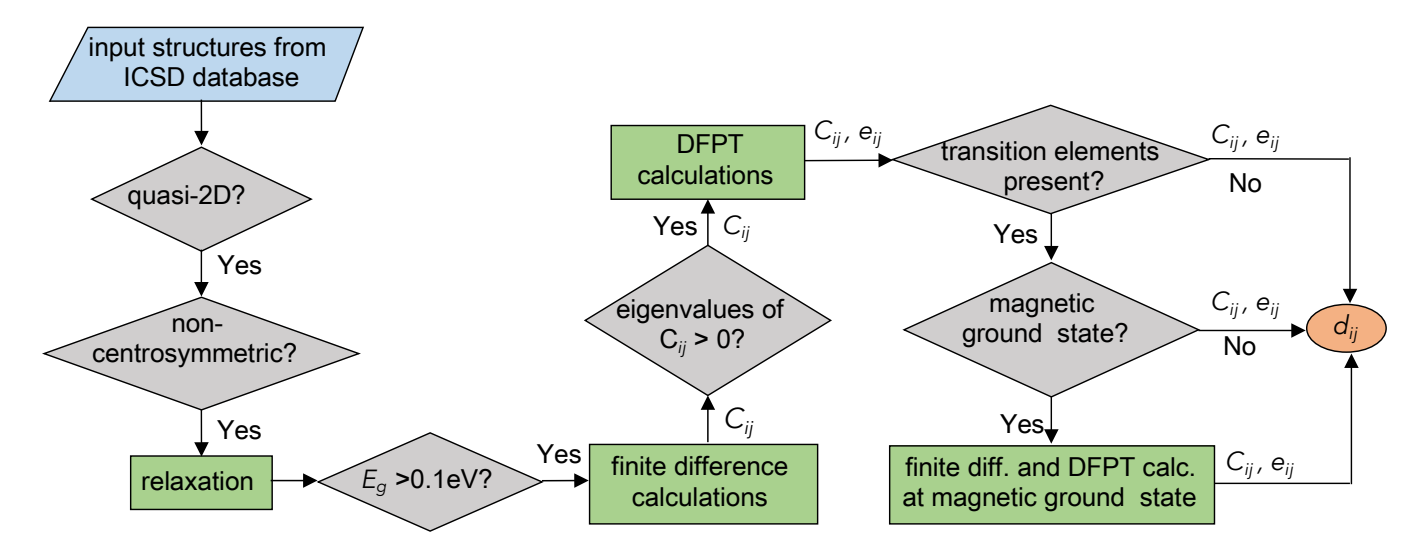


FIG. 4. Workflow for calculations of piezoelectric coefficient tensor e_{ij} , the elastic stiffness C_{ij} , and the piezoelectric modulus tensor d_{ij} of quasi-2D materials. A vdW-corrected functional (optB86) is used in all calculations. We have calculated piezoelectric modulus of 80 quasi-2D materials.

isons for predicted piezoelectric properties. In the supplemental information Table S1, we have provided the experimental details (*e.g.* measurement techniques, measuring temperatures, *etc.*) for each compound shown in Figure 3. The comparison of calculated and experimental values for the piezoelectric modulus of a few commercially important piezoelectric materials (including AIN and PbTiO 3) are shown supplementary information. Predicted piezoelectric moduli are found to be in good agreement with experimental values.

C. Workflow for identifying quasi-2D piezoelectrics

A complete workflow we developed for identifying promising quasi-2D piezoelectric materials is illustrated in Figure 4. The binary and ternary crystal tures from the ICSD database are first screened using the automated algorithm for identifying quasi-2D structures. Then, we filter out all centrosymmetric structures based on the space group assigned in ICSD. Out of ~11500 binary and ternary materials we find 869 layered systems, out of which 135 are identified as having non-centrosymmetric structures. Next. the noncentrosymmetric, structures are relaxed using the previously described first-principles calculations employing a vdW-corrected functional. As the piezoelectric materials need to have sizable band gaps for their properties to not be screened by the existence of free charge carriers we next employ a band-gap filter. As suggested in the previous works, 28,44 for electronic structure calculation, we perform self-consistent GGA-PBE calculations on the vdW-relaxed structures using dense k-point grids. Because of the known band gap error in DFT calculations we use a relatively generous band gap cutoff of 0.1 eV. Fifty additional materials with their band gap

smaller than 0.1 eV are discarded as a result. Finite difference calculations are performed with vdW-corrected functional to obtain the elastic constants (C). Five materials with elastic tensors with negative eigenvalues are also discarded. According to Born stability criteria, 45 the elastically stable materials always have positive eigenvalues of stiffness matrix. This means that an elastically stable materials always have positive elastic energy for arbitrary homogeneous deformation by an infinitesimal strain. 46 With the remaining 80 candidates, we proceed our calculations by performing Density Functional Perturbation Theory (DFPT) 37-39 calculations to assess their piezoelectric coefficient tensor, e. Out of the remaining 80 candidates, 38 materials contain transition metal elements. For these, we perform a limited search of the magnetic ground state by enumerating all magnetic configurations in the unit cell and calculating their total energies. The elastic and piezo calculations are then performed only on the lowest energy spin stateThis step is necessary because of the strong dependence of the electronic structure and other properties on spin configuration discussed in more details in Ref. 47. The automated DFT calculations including initial file generation, calculating properties, data extraction and data handling are performed with the help of PyLada, 48 a Python framework for high-throughput first-principles calculations.

III. RESULTS AND DISCUSSIONS

A. Promising Quasi-2D Piezoelectric Waterials

Based on the calculated piezoelectric modulus tensor, a number of candidate materials with relatively large d_{ij} components have emerged. They are shown in Figure 5 with the full list together with the corresponding d_{ij} , C_{ij}

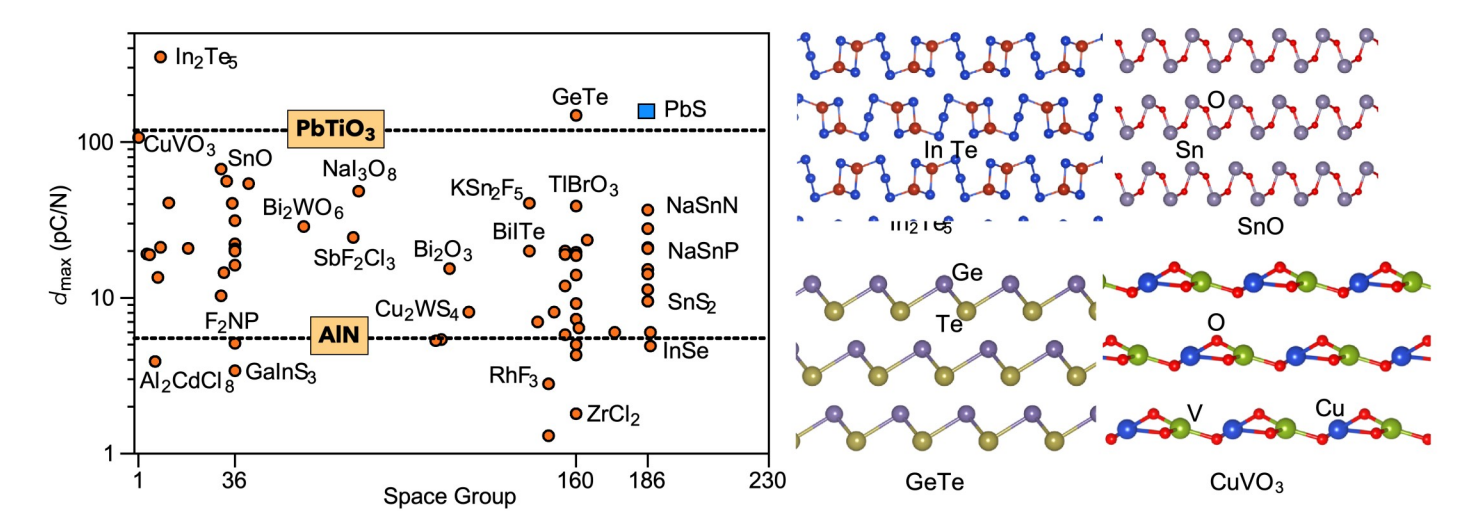


FIG. 5. Left panel: plot of $d_{max} = max(|d_{ij}|)$ against the space group number for 63 quasi-2D vdW materials with $d_{max} > 0$ (out of 135 non-centrosymmetric compounds). The two horizontal dotted lines denote the d_{33} values of PbTiO₃ (119 pC/N) and AlN (5.5 pC/N). The blue square in this plot represents the hypothetical structure of PbS (distorted NiAs found in ICSD), not the ground rocksalt structure. Right panel: crystal structures of quasi-2D materials with large piezoelectric moduli.

and e_{ij} values provided in the supplementary information. In addition, the top 20 most promising systems, based on the largest q component, are listed in Table I.

The piezoelectric modulus tensor (δ) is a third rank tensor, and any isotropic averaging scheme will—yield zero.⁴⁹ To rank these materials based on the merit of their piezoelectric response, we define $d_{\rm max} = max(|d_{ij}|)$ as the largest element of the absolute d_{ij} matrix. Then the $d_{\rm max}$ is plotted against the space group number in Figure 5. The two reference lines have been drawn for categorizing these candidates – one representing calculated d_{33} of PbTiO $_3$ and the other representing calculated d_{33} of AlN (see supplementary information for the benchmark agains experiments).

Please note that $PbTiO_3$ is also a ferroelectric and here we are only using the value for its piezoelectric response. More precisely, the $PbTiO_3$ reference line corresponds to the bulk piezoelectric modulus corresponding to the single-crystal single-domain samples.

The materials shown in the left panel of Figure 5 can broadly be divided in three categories. The first category is comprised of quasi-2D compounds with d_{max} larger than the longitudinal piezoelectric modulus of PbTiO $_3$ (d_{33} =119 pC/N) 1 – the key end member of most commercial high-strain piezoelectrics. We found three materials ($\ln_2 \text{Te}_5$, PbS, and GeTe) in this category. Among them PbS is not in its ground state rocksalt phase, but in the hypothetical distorted NiAs structure which has found its way into the ICSD. The other two compounds have previously been experimentally synthesized, 51,52 but their piezoelectric moduli have not been reported so far.

In the second category we group all compounds which have d_{nax} larger than the longitudinal piezoelectric modulus of AlN (d_{33} =5.5 pC/N) 53 and lower than the longitudinal piezoelectric modulus of PbTiO $_3$. The majority

(48 compounds) of the piezoelectric candidates from our study fall in this category revealing that overall the vdW bonded quasi-2D systems indeed exhibit a propensity toward large piezo-response. This group is composed from oxides and other chalcogenides such as CuVO₃, SnO, BilnO₃, MoV₂O₈, SnS₂, InSe, Cs₂Te₃ and other (total of 30); halides such as KS_{P₂}F₅, AgI, MgCl₂, and PbI₂ (total of 4); pnictides such as NaSnN, NaSnP, KSnAs, and NaN₃ (total of 4). Also, a number of materials in this group (10) are the mixed anion systems, e.g., Nal₃O₈, SbF₂Cl₃. Not surprisingly, the more ionic systems like oxides, halides and nitrides are more frequently found closer to the top of the range. Finally, two compounds Cs₂Te₃ and Bi₂WO₆ are found in calculations to be dynamically unstable, but both have been experimentally synthesized (likely high-temperature phases).54,55

The last group is composed of materials with the piezo-electric response lower than the longitudinal piezoelectric modulus of AlN. Though these candidates exhibit low piezoelectric response, they could still be useful as the calculated moduli are comparable with that of quartz (d_{11} =2.27 pC/N). ⁵⁶ We found a total of 12 compounds which fall in this category. Examples include: WS₂, RhF₃, ZrCl₂, and GalnS₃. The moduli δ , ϵ and $\mathcal C$ with other informations such as band gap, space group of these compounds are provided in the supplementary information.

We also observe that the piezoelectric compounds in the quasi-2D family of solids are clustered mainly in three specific space groups *i.e.*, space group no. 36 ($Cmc2_1$), 160 (R3m), and 186 ($P6_3mc$). This is mainly a reflection of the population bias, as these are the three most frequently occurring non-centrosymmetric space groups in the quasi-2D family of crystals.

Table I shows that in 9 of the high-response quasi-2D

TABLE I. List of top 20 candidate quasi-2D piezoelectric materials are shown with their space group (SG) number, calculated DFT band gap $(E \ g)$, maximal piezoelectric modulus d_{max} , the d_{ij} component that appears as d_{max} , maximal e_{ij} (e_{max}), the e_{max} component of e_{ij} .

Compound	SG	$E_g(eV)$	d _{max} (pC/N)	max d _{ij}	e _{max} (C/m ²)	max eij	$e_{d_{max}}$ (C/m 2)
In ₂ Te ₅	9	0.7	351.7	d ₁₅	2.6	e ₁₅	2.6
PbS^t	186	0.2	161.4	d_{33}	8.3	e_{33}	8.3
GeTe	160	0.6	148.4	d ₁₅	3.3	$e_{_{15}}$	3.3
CuVO ₃	1	0.9	106.9	d_{22}	0.8	e_{32}	0.2
SnO	31	1.6	67.1	d_{22}	1.1	e_{22}	1.1
BiInO 3	33	2.8	56.1	d_{33}	4.7	e_{33}	4.7
$Bi_2WO_6^{\sharp}$	41	1.7	54.1	d_{24}	3.9	e_{33}	2.9
Nal ₃ O ₈	81	2.8	48.4	d_{14}	0.7	e_{31}	0.6
NaN ₃	12	1.4	40.7	d_{36}	0.3	e_{34}	0.1
KSn_2F_5	143	3.0	40.5	d ₁₅	0.3	$e_{_{15}}$	0.3
MoV_2O_8	35	8.0	40.4	d_{33}	2.9	e_{33}	2.9
TIBrO 3	160	3.0	38.8	d_{24}	1.0	e_{24}	1.0
NaSnN	186	1.1	36.6	d ₁₅	0.6	$e_{_{15}}$	0.6
Cs ₂ Te ₃ [‡]	36	0.5	31.3	d_{36}	0.6	e_{11}	0.4
Bi_2MoO_6	61	1.7	28.7	d_{26}	1.6	e_{11}	1.3
Agl	186	1.3	27.8	d ₁₅	0.3	e_{33}	0.1
SbF ₂ Cl ₃	79	1.5	24.4	d ₁₅	0.2	e_{33}	0.1
MgCl ₂	115	4.9	23.5	d ₁₅	0.2	$e_{_{15}}$	0.2
$PbRb_2O_3$	36	1.3	22.2	d_{34}	0.7	e_{34}	0.7
BiGeO ₅	9	2.3	21.1	d ₃₃	3.0	e_{33}	3.0

[†] hypothetical structures

piezoelectric compounds,the d_{15} component appears as d_{max} . Note that because of the freedom in choosing the in-plane axes, d_{15} and d_{24} are virtually indistinguishable (see the discussion section)This component corresponds to the thickness shearing deformation where the material shears like a deck of cards in the in-plane direction, with no change in the other dimension. Materials with large d_{15} can be used in a variety of applications includingsensors, actuators, accelerometer, material testing structural health monitoring, non-destructive testing (NDT), and non-destructive evaluation (NDE). The components of d_{ij} appearing as d_{max} usually coincide with the components of d_{ij} appearing as d_{max} . The distribution of different components of d_{ij} (and e_{ij}) appearing as d_{max} (and e_{max}) are discussed in more detail in the next section.

Another quantity that could influence the piezoelectric response is the band gap of the material. In this work the band gaps are calculated at the DFT level and are also shown in Table I and supplementary information. Only about 1/3 of the studied materials are found to have DFT band gaps below 1 eV. Given the well known underestimation of band gaps in DFT based methods we do not think that materials with DFT band gaps larger than 1 eV would suffer from problems related to the existence of free charge carriers due to thermal fluctuations. However, for those with smaller gaps thermal fluctuation may cause sufficient number of free charge carriers, which may lower the polarization upon straining these materi-

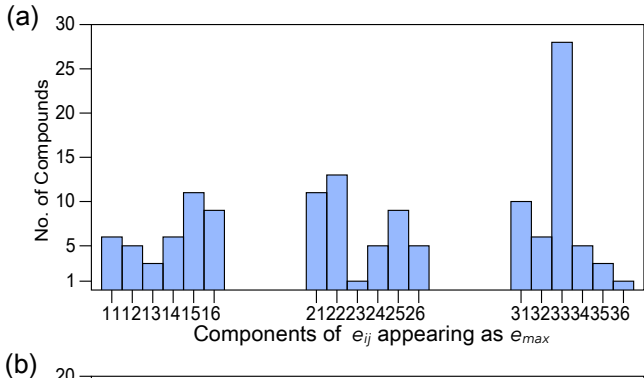
als despite having large piezoelectric moduli. Of course, provided that the real band gap is sufficiently close to the DFT one. For these materials, a more accurate assessment of the electronic structure might be needed before they are considered for applications.

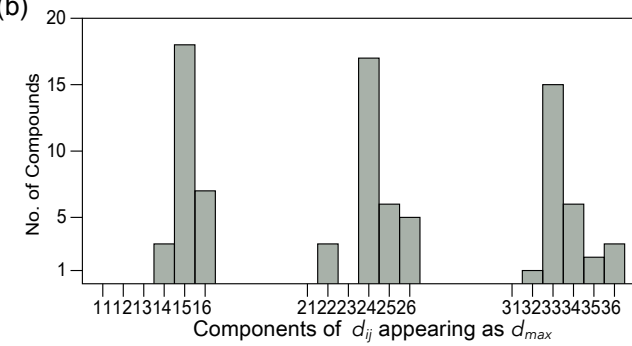
In relation to the chemical composition and toxicity it is also important to not that currently, the most widely used piezoelectric material is lead zirconate titanate (PbZr $_{1-x}$ Ti $_x$ O $_3$ or PZT). However, PZT causes significant environmental problems because of its high lead content. Hence, significant efforts have been made to develop lead-free piezoelectric materials. In our work, we have identified 44 candidates that do not contain any toxic elements including Pb. Out of 44 candidates, 33 of them have their piezoelectric modulus larger than AIN.

3. Role of van der Waals Interactions

In order to understand the role of van der Waals interactions on the piezoelectric response of quasi-2D materials, we analyze the relationships of e_{nax} and d_{max} to the corresponding strain and stress components, respectively. A histogram showing the number of compounds with a given e_{ij} component appearing as e_{ij} is shown in Figure 6 (a). We observe that the most frequent e_{nax} is e_{33} . This indicates that in the majority of quasi-2D ma-

[‡] dynamically unstable





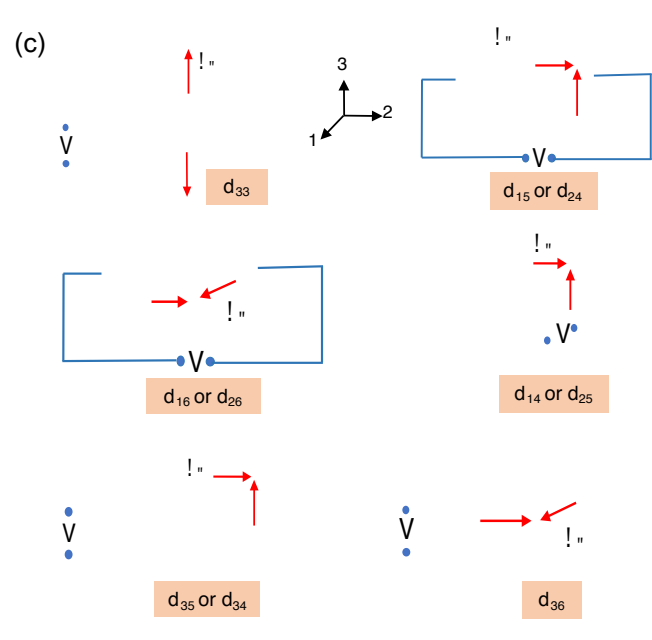


FIG. 6. Histogram of the maximum components of (a) the piezoelectric coefficient tensor, e_{max} and (b) piezoelectric modulus tensor, d_{nax} . The most frequent e_{nax} is e_{33} , whereas for d_{max} the most frequent maximum values are d_{15} , d_{24} and d_{33} . (c) Schematics of several important piezoelectric operating modes with their corresponding deformation types. The schematics of other relevant piezoelectric operating modes, *i.e.*, components of d_{ij} are shown in the supplementary information.

terials the largest piezoelectric response, as measured by the e_{ij} , is along the layer stacking direction. The reason for this behavior is that the relatively weak vdW inter-

actions allow large charge redistribution in the layering direction upon straining the system.

On the other hand, the piezoelectric modulus tensor δ relates relates stress to polarization and combines two types of effects: (1) amount of strain due to application of stress, and (2) amount of charge redistribution (polarization) due to resultant strain produced by the applied stress. A similar histogram of the d_{ij} components appearing as d_{max} is shown in Figure 6(b). We divide the d_{ii} components into three groups depending on the deformation types (stress components) and the polarization direction. The schematics of the polarization directions and the associated stress components is shown in Figure 6(c) together with the d ij components connecting the two. Every component of d_{ij} represents a separate piezoelectric operating mode. Schematics of all possible piezoelectric modes are provided in supplementary information.

Group I: Applied stress deforms van der Waals bonds and the measured polarization coincides with the direction of the deformations. The longitudinal mode (d_{33}) and shear modes (d_5 and d_{24}) fall in this class. As evident from the histogram in Figure 6(b) these are the most frequently appearing d_{max} components. In our considered materials, the modes d_{24} and d_{15} are indistinguishable because of the arbitrariness of the choice of axes '1' and '2', while the axis '3' is fixed by layer stacking directions. In both of these modes, the same stress component (σ_4) is responsible for the deformation, which implies shearing of the van der Waals gaps. On the other hand, in the d_{33} , the applied stress axially deforms (stretches or compresses) van der Waals gaps. Hence, the large piezoelectric responses are achieved by deforming (axial or shear) the relatively soft van der Waals bonds. The bar-heights of d_{15} and d_{24} in the histogram of d_{max} in Figure 6(b) are larger compared to d_{33} . This is because the shearing resistance values (4) of quasi-2D materials are lower compared to their axial resistance values (G₃) (refer to Figure 3(b)).

Group II: Applied stress deforms van der Waals bonds, but the measuring polarization directions are different from their deformation directions. The face shear modes $(d_{14} \text{ and } d_{25})$ and the thickness-extension modes $(\mathcal{A} \text{ and } d_{32})$ fall in this class. The schematics of d_{31} and d_{32} are provided in the supplementary information. Usually, the direction of polarization is facilitated by the direction of deformation. In such modes, the deformation directions are different from their measured polarization directions. This is the reason behind their low occurrence in the histogram of d_{max} though the van der Waals bond are deformed by the applied stress.

Group III: The van der Waals bond does not deform by the applied stress in these modes. This is why these modes do not appear frequently in the histogram of $n_{\rm dex}$. This includes length or width extension modes (d_{11} or d_{22}) and shearing modes of type d_{16} and d_{36} .

The above discussion implies that the large piezoelectric response is always accompanied and caused by the

stress that deforms the "soft" van der Waals gaps either through stretching, compression, or shearing. In addition, the analysis of the maximal piezoelectric moduli and the associated stress components provided guidance to experimentalists of how thin films should be grown to utilize large d_{max} . It also describes what kind of mechanical actuation is necessary to achieve large piezoelectric response. This also helps in the design of new devices to take advantage of large d_{max} . Finally, these findings can open up a wide variety of devices based on their operation modes or based on new materials for nonconventional modes. For example, materials with large face-shear (d_4) mode response will be attractive for for torsional applications, like novel gyroscopic sensors or high-precision torsional MEMS actuators. ⁵⁷

C. Axial Piezoelectric and €lastic Anisotropy

In addition to revealing new candidate piezoelectric materials and explaining the origin of strong piezoelectric response, we have also investigated the anisotropy in axial piezoelectric response in relation to the axial elastic anisotropy. We analyze how the response in the out-ofplane direction compares to the in-plane responses. The in-plane and out-of-plane directions in quasi-2D materials are trivial to define and are illustrated in Figure 1. We define the axial anisotropy in both elastic and piezoelectric responses by the ratio of the out-of-plane component to the in-plane component. Here, the in-plane component is defined by the arithmetic mean of the '11' and '22'components (invariant to the choice of the in-plane axes). whereas the out-of-plane response is solely defined by the '33'-component. Hence, the axial anisotropy of δ , ϵ , and \mathbb{C} can be expressed as $2\mathfrak{g}/(d_{11}+d_{22})$, $2e_{33}/(e_{11}+e_{22})$, and $2C_{33}/(C_{11}+C_{22})$ respectively. If the axial anisotropy equals or nearly equals 1 then the material is considered to be isotropic in the corresponding quantity responses with respect to the in-plane and out-of-plane directions. If the axial anisotropy is greater (or lower) than 1 the response of a material to axial deformation is dominated in out-of-plane (in-plane) direction.

All possible correlations among the axial anisotropy of δ , ε , and $\mathbb C$ have been investigated. The correlation between axial anisotropy of δ with respect to the axial anisotropy of ε and $\mathbb C$ are shown in Figure 7 (a) and (b) respectively. From the comparative studies between Figure 7 (a) and (b), we see that the axial anisotropy of δ is mainly dictated by the axial anisotropy of ε not by the axial anisotropy of $\mathbb C$. The plot between axial anisotropy of $\mathbb C$ and ε is provided in the supplementary information.

From Figure 7 (a) and (b), we observe that most quasi-2D materials have axial piezoelectric anisotropy parameter (both in δ and \mathfrak{e}) > 1 and axial elastic anisotropy parameter < 1. This implies that the quasi-2D piezoelectric materials are dominant in out-of-plane piezoelectric responses but elastically they are dominant in-plane directions. This result corroborates the correla-

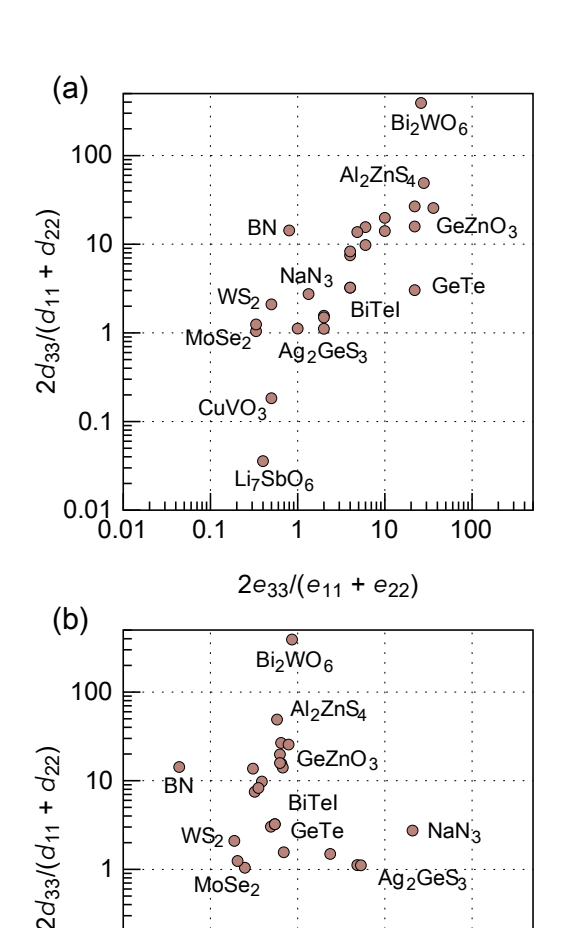


FIG. 7. Correlation between axial anisotropy, *i.e.*, out-of-plane to in-plane response ratio) of (a) δ and ε (b) δ and $\mathbb C$. The results reveal that majority of quasi-2D piezoelectric materials are dominated by out-of-plane piezoelectric responses (both in ε and δ) but elastically they are dominated in in-plane direction.

Li₇SbO₆

 $2C_{33}/(C_{11} + C_{22})$

0.1

0.01 <u></u> 0.01

0.1

CuVO₃

10

100

tion between elastic softness and large piezoelectric response, *i.e.*, the large piezoelectric responses are observed in elastically softer directions. We found quasi-2D piezoelectric compounds such as CuVQand Li₇SbQ₆ are dominated by in-plane piezoelectric response. Compounds such as Bi₂WO₆, Al₂ZnS₄, GeZnO₃, and GeTe are nearly isotropic in their axial elastic responses but highly anisotropic in axial piezoelectric responses.

iv. conclusions

In conclusion, we performed a large-scale computational (first-principles) assessment of the bulk piezoelec-

tric properties of layered (quasi-2D), vdW bonded materials. In our study we concentrate on the piezoelectric modulus as the measure of the piezoelectric response, which relates mechanical stress and electric polarization and depends on a combination of charge redistribution due to strain and the amount of strain produced by the stress. Overall, out of 135 non-centrosymmetric quasi-2D binary and ternary structures from ICSD we have discovered 51 materials with piezoelectric response larger than that of AIN, a well-known piezoelectric materials used in applications. Out of these 51 systems, we find three with the piezoelectric modulus even larger than that of PbTiO 3 that has the piezoelectric modulus among the largest known. More importantly, 33 out of the 51 layered compounds do not contain any toxic elements including

Pb. Our results also reveal that the large piezoelectric modulus in vdW systems is directly enabled by the vdW interactions between layers as in majority of compounds the large components of the piezoelectric modulus tensor couple to the stress components that imply deformations (both shear and axial) of the "soft" vdW bonds between layers. Our results suggest that quasi-2D layered materials are a rich structural space for discovering new piezoelectric materials.

Acknowledgement The authors gratefully acknowledge the support of the National Science Foundation through Grant No. DMREF-1534503. The calculations were performed using the high-performance computing facilities at National Renewable Energy Laboratory (NREL) and at Colorado School of Mines (the Golden Energy Computing Organization).

- ¹ B. Jaffe, *Piezoelectric Ceramics*, Non-Metallic Solids (Elsevier Science, 2012).
- ² K. Uchino, *Piezoelectric Actuators and Ultrasonic Motors*, Electronic Materials: Science & Technology (Springer US, 1996).
- ³ S. Liu, L. Wang, Z. Wang, Y. Cai, X. Feng, Y. Qin, and Z. L. Wang, ACS Nano 12, 1732 (2018), https://doi.org/10.1021/acsnano.7b08447.
- ⁴ R. Weigel, D. P. Morgan, J. M. Owens, A. Ballato, K. M. Lakin, K. Hashimoto, and C. C. W. Ruppel, IEEE Transactions on Microwave Theory and Techniques 50, 738 (2002).
- W. Wu and Z. L. Wang, Nature Reviews Materials 1, 16031 (2016).
- ⁶ K. Uchino, Smart Materials and Structures *7*, 273 (1998).
- Y. Saito, H. Takao, T. Tani, T. Nonoyama, K. Takatori, T. Homma, T. Nagaya, and M. Nakamura, Nature 432, 84 (2004).
- ⁸ R. Armiento, B. Kozinsky, G. Hautier, M. Fornari, and G. Ceder, Physical Review B 89, 134103 (2014).
- ⁹ R. Armiento, B. Kozinsky, M. Fornari, and G. Ceder, Physical Review B 84, 014103 (2011).
- M. De Jong, W. Chen, H. Geerlings, M. Asta, and K. A. Persson, Scientific Data 2 (2015).
- ¹¹ L. Dong, J. Lou, and V. B. Shenoy, ACS Nano 11, 8242 (2017).
- ¹² M. N. Blonsky, H. L. Zhuang, A. K. Singh, and R. G. Hennig, ACS Nano 9, 9885 (2015).
- ¹³ W. Li and J. Li, Nano Research 8, 3796 (2015).
- ¹⁴ H. Yin, J. Gao, G. P. Zheng, Y. Wang, and Y. Ma, The Journal of Physical Chemistry C 121, 25576 (2017).
- ¹⁵ K.-A. N. Duerloo, M. T. Ong, and E. J. Reed, The Journal of Physical Chemistry Letters 3, 2871 (2012).
- ¹⁶ R. Hinchet, U. Khan, C. Falconi, and S.-W. Kim, Materials Today (2018).
- J. F. Nye, Physical properties of crystals: their representation by tensors and matrices (Oxford University Press, 1985).
- "We refer ε, which couple strain and electric displacement as piezoelectric coefficient tensor or piezoelectric stress coefficients. δ, which couple stress with electric displacement, are referred to as piezoelectric modulus tensor or piezoelec-

- tric strain modulus. in both cases, we express the individual matrix elements in standard reduced voigt notation,".
- W. Voigt, Lehrbuch der kristallphysik (mit ausschluss der kristalloptik) (Springer-Verlag, 2014).
- ²⁰ R. Lec and W. Soluch, in *Ultrasonics Symposium*, 1977 (IEEE, 1977) pp. 389–392.
- A. Pramanick, D. Damjanovic, J. E. Daniels, J. C. Nino, and J. L. Jones, Journal of the American Ceramic Society 94, 293 (2011).
- ²² Z. Li, M. Grimsditch, X. Xu, and S. K. Chan, Ferroelectrics 141, 313 (1993).
- ²³ K. Lefki and G. Dormans, Journal of Applied Physics 76, 1764 (1994).
- ²⁴ A. V. Sotnikov, H. Schmidt, M. Weihnacht, E. P. Smirnova, T. Y. Chemekova, and Y. N. Makarov, IEEE transactions on ultrasonics, ferroelectrics, and frequency control 57 (2010).
- ²⁵ Z.-G. Ye, Handbook of advanced dielectric, piezoelectric and ferroelectric materials: Synthesis, properties and applications (Elsevier, 2008).
- G. Bergerhoff, R. Hundt, R. Sievers, and I. Brown, Journal of Chemical Information and Computer Sciences 23, 66 (1983).
- A. Belsky, M. Hellenbrandt, V. L. Karen, and P. Luksch, Acta Crystallographica Section B: Structural Science 58, 364 (2002).
- P. Gorai, E. S. Toberer, and V. Stevanovi´c, Journal of Materials Chemistry A 4, 11110 (2016).
- ²⁹ M. Ashton, J. Paul, S. B. Sinnott, and R. G. Hennig, Physical Review Letter 118, 106101 (2017).
- N. Mounet, M. Gibertini, P. Schwaller, D. Campi, A. Merkys, A. Marrazzo, T. Sohier, I. E. Castelli, A. Cepellotti, G. Pizzi, and N. Marzari, Nature Nanotechnology , 1 (2018).
- 31 G. Cheon, K.-A. N. Duerloo, A. D. Sendek, C. Porter, Y. Chen, and E. J. Reed, Nano Letters 17, 1915 (2017).
- ³² S. Leb`egue,T. Bj'orkman, M. Klintenberg, R. M. Nieminen, and O. Eriksson, Physical Review X 3, 031002 (2013).
- ³³ G. Kresse and J. Hafner, Physical Review B 47, 558 (1993).
- ³⁴ G. Kresse and J. Furthmüller, Physical Review B 54, 11169 (1996).
- ³⁵ J. c. v. Klime's, D. R. Bowler, and A. Michaelides, Physical

- Review B 83, 195131 (2011).
- ³⁶ J. Klime's, D. R. Bowler, and A. Michaelides, Journal of Physics: Condensed Matter 22, 022201 (2009).
- ³⁷ S. Baroni, S. De Gironcoli, A. Dal Corso, and P. Giannozzi, Reviews of Modern Physics 73, 515 (2001).
- ³⁸ S. Baroni, P. Giannozzi, and A. Testa, Physical Review Letter 58, 1861 (1987).
- 39 X. Gonze, Physical Review A 52, 1096 (1995).
- ⁴⁰ Y. Le Page and P. Saxe, Physical Review B 65, 104104 (2002).
- ⁴¹ B. Narayanan, I. E. Reimanis, E. R. Fuller Jr, and C. V. Ciobanu, Physical Review B 81, 104106 (2010).
- ⁴² J. P. Perdew, K. Burke, and M. Ernzerhof, Physical Review Letter 77, 3865 (1996).
- ⁴³ A. Jain, S. P. Ong, G. Hautier, W. Chen, W. D. Richards, S. Dacek, S. Cholia, D. Gunter, D. Skinner, G. Ceder, and K. A. Persson, APL Materials 1, 011002 (2013), https://doi.org/10.1063/1.4812323.
- ⁴⁴ N. Marom, A. Tkatchenko, M. Scheffler, and L. Kronik, Journal of Chemical Theory and Computation 6, 81 (2009).
- ⁴⁵ M. Born, in *Mathematical Proceedings of the Cambridge Philosophical Society*, Vol. 36 (Cambridge University Press, 1940) pp. 160–172.
- ⁴⁶ F. Mouhat and F.-X. Coudert, Physical Review B 90, 224104 (2014).
- ⁴⁷ P. Gorai, E. S. Toberer, and V. Stevanovi c, Physical Chemistry Chemical Physics 18, 31777 (2016).
- ⁴⁸ Pylada:, "A python framework for high-throughput first-

- principles calculations," https://github.com/pvlada.
- ⁴⁹ J. Y. Li, Journal of the Mechanics and Physics of Solids 48, 529 (2000).
- D. Zagorac, K. Doll, J. C. Schön, and M. Jansen, Physical Review B 84, 045206 (2011).
- ⁵¹ T. Chattopadhyay, J. X. Boucherle, and H. G. vonSchnering, Journal of Physics C: Solid State Physics 20, 1431 (1987).
- ⁵² H. Sutherland, J. Hogg, and P. Walton, Acta Crystallographica Section B: Structural Crystallography and Crystal Chemistry 32, 2539 (1976).
- M.-A. Dubois and P. Muralt, Applied Physics Letters 74, 3032 (1999).
- ⁵⁴ K. Chuntonov, A. Orlov, S. Yatsenko, Y. N. Grin, and L. Miroshnikova, Izv. Akad. Nauk SSSR, Neorg. Mater 18, 1113 (1982).
- ⁵⁵ R. Wolfe, R. Newnahm, and M. Kay, Solid State Communications 7, 1797 (1969).
- ⁵⁶ V. E. Bottom, Journal of Applied physics 41, 3941 (1970).
- ⁵⁷ G. Boivin, P. B'elanger, and R. J. Zednik, in *THERMEC* 2016, Materials Science Forum, Vol. 879 (Trans Tech Publications, 2017) pp. 637–641.
- ⁵⁸ T. R. Shrout and S. J. Zhang, Journal of Electroceramics 19, 113 (2007).
- ⁵⁹ T. Takenaka and H. Nagata, Journal of the European Ceramic Society 25, 2693 (2005).
- ⁶⁰ P. Baettig, C. F. Schelle, R. LeSar, U. V. Waghmare, and N. A. Spaldin, Chemistry of materials 17, 1376 (2005).